GSA Data Repository 2020042

Lehmann, B., et al., 2020, Postglacial erosion of bedrock surfaces and deglaciation timing: New insights from the Mont Blanc massif (western Alps): Geology, v. 48, https://doi.org/10.1130/G46585.1

Appendix DR1: Sample preparation, measurement and analysis

For every sample, both OSL and ^{10}Be surface exposure dating analysis were performed.

The method of ^{10}Be sample preparation is comprehensively described in the literature (e.g., Kohl and Nishiizumi, 1992; Ivy-Ochs, 1996). We use grain sizes in between 250 µm and 1 mm of quartz separates. The addition of a commercial ^{9}Be carrier is followed by quartz dissolution in HF and Be purification using ion-exchange columns and selective precipitation. The ^{10}Be/^{9}Be ratio was measured by accelerator mass spectrometry (AMS) on the 600 KV TANDY system at the Laboratory of Ion Beam Physics (LIP) at ETH Zürich. The results have been normalized to the ETH Zurich in-house Be-10 standard S2007N with a nominal value of ^{10}Be/^{9}Be = 28.1 × 10^{-12} (Christl et al., 2013). S2007N has been calibrated relative to the ICN 01-5-1 standard using a nominal value of ^{10}Be/^{9}Be = 2.709 × 10^{-11} (Nishiizumi et al., 2007). We correct for a long-term average full chemistry procedural blank of ^{10}Be/^{9}Be = (3.7 ± 2.2) × 10^{-15}. Ages are calculated using the local production rate of the Chironico landslide: 4.16 ± 0.10 at g_{quartz}^{-1} a^{-1}, with the Lifton-Sato-Dunai (LSD) scaling scheme (Lifton et al., 2014), the ERA40 atmospheric model (Uppala et al., 2005) and the Lifton VDM 2016 geomagnetic database (for ages in between 0-14 ka, Pavon-Carrasco et al., 2014 and for ages in between 14-75 ka, GLOPIS-75, Laj et al., 2004) with a modified version of the CREp online calculator (Martin et al., 2016) to process non-linear erosion rate correction by solving Equation 3 in Lehmann et al., in press. The reported errors propagate uncertainties from AMS standard reproducibility, counting statistics, standard mean error of samples, blank correction and the local production rate value. These external errors are

used to compare absolute ages to independent chronologies. Internal errors exclude the uncertainty of the local production rate. All errors are reported on the 1s level.

For luminescence analysis, the bedrock samples were cored down to 30 mm depth using a Husqvarna DM220 drill, with 10-mm diameter. Cores were then sliced into 0.7-mm thick rock slices with a BUEHLER IsoMet low speed saw equipped with a 0.3-mm thick diamond blade. The samples were drilled and sliced under wet conditions (water and lubricant, respectively) to avoid any heating that could potentially reset the OSL signal. Sample preparation was done under subdued red-light conditions. The thickness of each rock slice was measured to determine the precise depth of each luminescence measurement. Luminescence measurements were performed using Risø TL-DA 20 TL/OSL readers (Bøtter-Jensen et al., 2010) equipped with ^{90}Sr beta sources at the University of Lausanne (Switzerland). We performed a preheat at 250°C before giving infrared (IR) stimulation (870 nm, FWHM 40 nm) at 50°C. The calculation of $\dot{D}$ was achieved through the measurement of the concentrations of U, Th, K and Rb of the bulk rock sample and the use of the DRAC online calculator (Table 2; Durcan et al., 2015) assuming a grain size between 750 and 1000 µm and water content of 2%. We use $\overline{\sigma\varphi}_0$ = 129 a^{-1} and μ = 0.596 mm^{-1} that were determined from two calibration rock surfaces of similar granitic lithology from the Mont Blanc massif, exhibit no erosion and have known exposure age, following the protocol presented in Lehmann et al. (2018). The calibration is presented in Fig. A2. The determination of D_0 was done by constructing dose response curves (DRC) of the IRSL signal measured at 50°C using a single aliquot regenerative dose (SAR) protocol (Murray and Wintle, 2000; Wallinga et al., 2000) and fitting the DRC with single saturating exponential. The validity of the measurement protocol was confirmed using a dose-recovery experiment (Wallinga et al., 2000). Recovered doses were within 10% of unity.

Table DR1: Sample list with their characteristics and measured ^{10}Be concentrations

Sample ID	Latitude	Longitude	Elevation	Thickness	Topographic	Surface	Lichen	^{10}Be conc.[a]	P(0) local[b]	Ḋ spec.[c]
	WGS 84		[m.a.s.l.]	cm	Shielding factor	orientation	% of cov.	[at g_{qtz}^{-1}]	[at g_{qtz}^{-1}]	[Gy a^{-1}]
Moine transect										
MBAM1	45.9094	6.9527	2447	7	0.758	135 W 65	0.8	264530 ± 11640	28.17 ± 0.68	7.7×10^{-3}
MBAM2	45.9087	6.9521	2363	2	0.79	152 W 12	0.2	262870 ± 11190	26.51 ± 0.64	7.9×10^{-3}
MBAM3	45.9082	6.9507	2259	4	0.698	170 W 70	0.8	218400 ± 9720	24.58 ± 0.59	7.3×10^{-3}
Trélaporte transect										
MBTP1	45.9083	6.9311	2545	8	0.963	140 E 18	0.7	474750 ± 17530	30.20 ± 0.73	7.4×10^{-3}
MBTP2	45.9086	6.9319	2460	8.5	0.949	14 E 27	0.6	403210 ± 17020	28.43 ± 0.69	7.3×10^{-3}
MBTP5	45.9112	6.9324	2220	8	0.926	108 SE 18	0.9	446710 ± 19740	23.88 ± 0.58	7.7×10^{-3}
MBTP6	45.9130	6.9327	2094	7	0.594	334 E 80	0.7	84100 ± 13160	21.75 ± 0.52	8.4×10^{-3}
MBTP9	45.9124	6.9330	2133	6	0.656	148 E 73	0.6	160300 ± 8180	22.39 ± 0.54	7.0×10^{-3}
MBTP11	45.9108	6.9315	2310	7	0.898	130 E 48	0.8	330490 ± 13010	25.51 ± 0.61	8.1×10^{-3}

(a) Measured against standard 07KNSTD (Nishiizumi et al., 2007), corrected for full process blank of $(3.7 \pm 2.2) \times 10^{-15}$ ^{10}Be/^{9}Be. (b) Local production rate of the Chironico landslide: 4.15 ± 0.10 at g^{-1} a^{-1} rescaled for every longitude (Claude et al., 2014), latitude and elevation and considering no erosion correction, with the LSD scaling scheme (Lifton et al., 2014), the ERA40 atmospheric model (Uppala et al., 2005) and the Lifton VDM 2016 geomagnetic database (for ages in between 0-14 ka, Pavon-Carrasco et al., 2014 and for ages in between 14-75 ka, GLOPIS-75, Laj et al., 2004). (c) Dose rates were calculated using the concentrations of U, Th, K and Rb of the bulk rock sample and the DRAC online calculator (details in Table A5; Durcan et al., 2015).

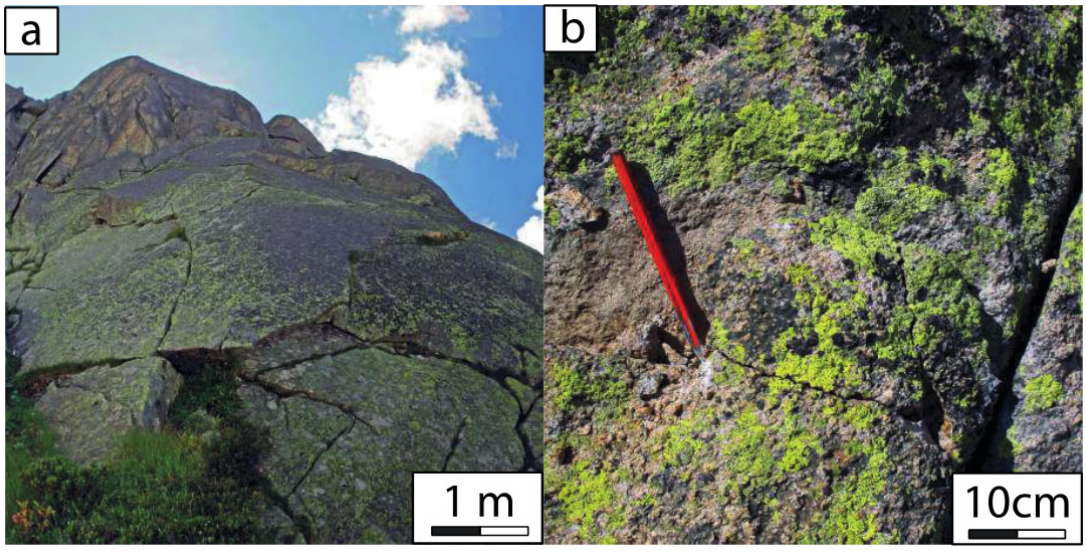

Figure DR1: Example of the glacially eroded bedrock surfaces sampled at two different scales (in this case surface MBTP5 from the Trélaporte profile)

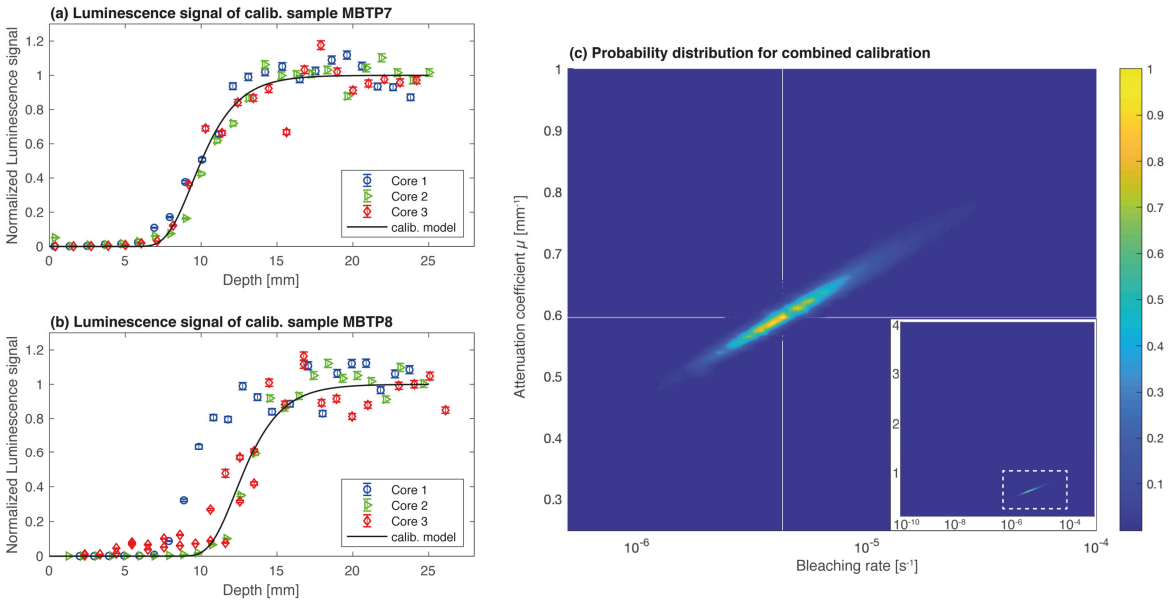

Figure DR2: Calibration of the parameters μ and $\overline{\sigma\varphi}_0$ using two calibration samples, MBTP7 (1936ma.s.l.) and MBPT8 (1995ma.s.l.), with exposure ages of 2 ± 2 years and 11 ± 2 years, respectively. These samples were at the bottom of the Trélaporte vertical profiles in 2016. The surfaces are located between the present-day position of the glacier and the Little Ice Age maximal elevation. These ages were determined using the reconstruction from Vincent et al. (2014). The calibration is made through an inversion protocol by prediction luminescence signals corresponding to the combinations of 10^4 values of $\overline{\sigma\varphi}_0$ in the logarithmic space and 10^4 values of μ. The inversed solutions are inferred using a least absolute deviation regression as described in Lehmann et al. (2018). The inferred calibrated values are μ = 0.596 mm^{-1} and $\overline{\sigma\varphi}_0$ = 129 a^{-1} (~ 4.08 × 10^{-6} s^{-1}).

Table DR2: TCN and OSL surface ages and inversion results for all surfaces

Sample ID	TCN age t_0 [1]	TCN age corr. tc_{ss} [2]	TCN age corr. tc_{max} [2]	OSL-surf. age [3]	t_s at SS	$\dot{\varepsilon}$ at SS	t_s max	$\dot{\varepsilon}$ max	t_s min	$\dot{\varepsilon}$ min
	[a]	[a]	[a]	[a]	[a]	[mm a^{-1}]	[a]	[mm a^{-1}]	[a]	[mm a^{-1}]
MBTP1	16428 ± 588	16647 ± 593	16657 ± 592	618 ± 147	2610	3.5×10^{-3}	20920	3.5×10^{-3}	-	-
MBTP2	15144 ± 609	15406 ± 625	15847 ± 649	606 ± 144	3146	3.5×10^{-3}	20920	3.5×10^{-3}	-	-
MBTP5	20227 ± 844	20838 ± 862	134090 ± 5852	4.6 ± 0.8	64	3.0×10^{-1}	3998	3.0×10^{-1}	20	7.0×10^{-1}
MBTP6	6667 ± 965	6830 ± 980	68692 ± 10617	0.4 ± 0.04	4	4.3	344	4.3	3	4.9
MBTP9	10970 ± 535	11212 ± 539	16523 ± 817	54 ± 14	486	3.2×10^{-2}	19510	3.2×10^{-2}	-	-
MBTP11	14482 ± 546	14987 ± 564	132250 ± 5101	3.4 ± 0.6	42	5.3×10^{-1}	2673	5.3×10^{-1}	-	-
MBAM1	12485 ± 546	12817 ± 593	45742 ± 2149	34 ± 8	285	5.7×10^{-2}	22200	5.7×10^{-2}	-	-
MBAM2	12157 ± 520	12411 ± 530	17993 ± 734	67 ± 16	461	2.8×10^{-2}	2162	2.8×10^{-2}	-	-
MBAM3	12543 ± 548	-	12780 ± 555	12 ± 2	-	-	56.92	2.0×10^{-1}	3	3.7

73

74 [1] Ages are calculated using the sea level high latitude (SLHL) rescaled local production rate of
75 the Chironico landslide: 4.15 ± 0.10 at g^{-1} a^{-1} rescaled for every longitude (Claude et al., 2014),
76 latitude and elevation and considering no erosion correction, with the LSD scaling scheme (Lifton
77 et al., 2014), the ERA40 atmospheric model (Uppala et al., 2005) and the Lifton VDM 2016
78 geomagnetic database (for ages in between 0-14 ka, Pavon-Carrasco et al., 2014 and for ages in
79 between 14-75 ka, GLOPIS-75, Laj et al., 2004) by solving Eq. (3). (2) TCN age corr. tc_{max}
80 correspond to the maximum corrected TCN exposure ages calculating from the best maximum 5%
81 solution. For (1) and (2) the errors represent the internal errors. (3) Ages were inverted using Eq.
82 (2) and prescribing 10^6 solutions for a range of time from 0 to t_0 (TCN age calculated using the
83 ^{10}Be concentration of each sample and solving Eq. (3) in Lehmann et al., 2019; without erosion
84 correction). All models were calculated using the following parameters: $\overline{\sigma\varphi}_0$ = 129 a^{-1}, μ = 596
85 m^{-1} and D_0 = 500 Gy. Specific $\dot{D}$ are show in Table A. A5. *SS means steady state.

86

87 Table DR3: Infrared stimulated luminescence at 50°C (IRSL50) experimental values of Trélaporte
88 profile

MBTP1

C1			C2			C3		
x [mm]	Lx/Tx	Lx/Tx Err.	x [mm]	Lx/Tx	Lx/Tx Err.	x [mm]	Lx/Tx	Lx/Tx Err.
1.81	0.00	0.000	2.24	0.00	0.000	1.97	0.00	0.005
2.80	0.00	0.000	3.16	0.00	0.001	2.91	0.00	0.001
3.76	0.00	0.001	4.14	0.00	0.001	3.96	0.00	0.000
4.70	0.00	0.001	5.09	0.00	0.001	4.99	0.00	0.001
5.72	0.00	0.001	6.07	0.00	0.001	5.95	0.00	0.001
6.80	0.00	0.001	7.10	0.00	0.000	6.85	0.00	0.002
7.77	0.00	0.002	8.04	0.00	0.001	7.72	0.01	0.003
8.68	0.00	0.002	8.89	0.00	0.001	8.62	0.01	0.007
9.52	0.00	0.001	9.77	0.00	0.002	9.54	0.03	0.013
10.49	0.01	0.003	10.72	0.01	0.002	10.42	0.02	0.004
11.53	0.01	0.002	11.70	0.01	0.003	11.36	0.04	0.022
12.49	0.01	0.002	12.64	0.02	0.008	12.32	0.07	0.011
13.47	0.01	0.006	13.63	0.05	0.010	13.65	0.19	0.109
14.41	0.02	0.018	14.63	0.13	0.175	15.00	0.24	0.073
15.56	0.02	0.014	15.60	0.11	0.032	15.95	0.26	0.100
17.02	0.03	0.005	16.76	0.15	0.072	16.88	0.55	0.193
18.25	0.14	0.176	17.93	0.14	0.127	17.79	0.63	0.109
19.24	0.15	0.149	19.19	0.36	0.091	18.73	0.83	0.171
20.30	0.16	0.108	20.38	0.50	0.101	19.65	0.87	0.150
21.23	0.24	0.179	21.29	0.74	0.125	20.82	0.79	0.165
22.16	0.47	0.348	22.30	0.88	0.118	21.98	0.92	0.136
			23.45	0.97	0.139	22.89	0.91	0.073
			24.59	1.00	0.082	23.86	1.00	0.082

MBTP2

C1			C2			C3		
x [mm]	Lx/Tx	Lx/Tx Err.	x [mm]	Lx/Tx	Lx/Tx Err.	x [mm]	Lx/Tx	Lx/Tx Err.
2.20	0.00	0.000	3.25	0.00	0.000	3.06	0.00	0.001
3.17	0.00	0.001	4.04	0.00	0.000	4.52	0.00	0.001
4.20	0.00	0.001	4.97	0.01	0.009	5.53	0.01	0.015
5.18	0.04	0.045	5.93	0.01	0.010	6.39	0.00	0.001
6.22	0.01	0.004	6.96	0.01	0.008	7.32	0.01	0.005
7.41	0.02	0.020	7.93	0.01	0.009	8.39	0.02	0.002
8.50	0.02	0.021	8.83	0.04	0.030	9.33	0.02	0.004
9.47	0.01	0.005	9.74	0.02	0.006	10.40	0.05	0.017
10.47	0.06	0.006	10.64	0.04	0.009	11.46	0.13	0.003
11.51	0.01	0.003	11.48	0.09	0.001	12.70	0.06	0.015
12.60	0.05	0.019	12.43	0.06	0.003	13.87	0.40	0.338
13.71	0.06	0.022	13.50	0.07	0.021	14.85	0.17	0.196
14.66	0.09	0.039	14.46	0.06	0.040	15.88	0.46	0.270
15.86	0.15	0.069	15.38	0.25	0.207	16.94	0.47	0.341
17.86	0.07	0.046	16.60	0.35	0.290	18.00	0.24	0.139
19.62	0.34	0.310	18.06	0.47	0.102	18.96	0.41	0.237
20.60	0.51	0.107	19.17	0.60	0.113	19.95	0.67	0.527
21.58	0.35	0.259	20.06	0.61	0.375	21.32	0.90	0.055
22.53	0.43	0.22	21.00	0.78	0.057	22.64	0.83	0.058
23.53	0.58	0.044	22.08	0.94	0.016	23.59	0.97	0.060
24.58	0.96	0.260	23.12	0.96	0.037	24.59	1.00	0.111
25.63	1.00	0.164	23.98	1.00	0.041			
26.63	0.96	0.023						

MBTP5

C1			C2			C3		
x [mm]	Lx/Tx	Lx/Tx Err.	x [mm]	Lx/Tx	Lx/Tx Err.	x [mm]	Lx/Tx	Lx/Tx Err.
3.86	0.01	0.000	3.86	0.01	0.000	2.15	0.01	0.000
6.45	0.06	0.001	4.99	0.04	0.001	3.09	0.01	0.000
7.94	0.25	0.005	6.45	0.04	0.003	4.03	0.01	0.000
9.46	0.31	0.007	7.94	0.06	0.002	4.97	0.05	0.001
10.67	0.70	0.015	9.46	0.38	0.010	5.91	0.06	0.001
11.70	0.87	0.019	10.67	0.21	0.005	6.87	0.19	0.004
12.90	1.00	0.021	11.70	0.23	0.005	7.87	0.17	0.004
13.95	1.00	0.021	12.90	0.46	0.012	8.89	0.27	0.006
15.03	0.99	0.021	13.95	0.39	0.011	9.89	0.20	0.004
16.08	0.94	0.020	15.03	0.82	0.020	10.84	0.21	0.005
17.08	0.98	0.021	16.08	0.88	0.021	11.74	0.50	0.011
18.34	1.00	0.022	17.08	1.02	0.024	12.66	0.46	0.011
19.55	1.03	0.022	18.34	0.72	0.019	13.63	1.05	0.023
20.56	1.05	0.023	19.55	1.01	0.028	14.69	1.06	0.023
21.50	0.89	0.019	20.56	0.91	0.021	15.72	0.80	0.019
22.46	0.91	0.020	21.50	0.95	0.021	16.68	0.98	0.022
23.43	1.16	0.025	22.46	1.10	0.025	17.57	0.93	0.020
24.42	1.04	0.022	23.43	1.13	0.025	18.42	1.02	0.022
			24.42	0.96	0.022	19.32	1.16	0.025
			25.51	0.95	0.021			
			26.61	0.92	0.020			
			27.78	1.17	0.026			

MBTP6

C1			C2			C3		
x [mm]	Lx/Tx	Lx/Tx Err.	x [mm]	Lx/Tx	Lx/Tx Err.	x [mm]	Lx/Tx	Lx/Tx Err.
1.96	0.00	0.000	1.96	0.01	0.000	3.32	0.01	0.000
3.00	0.01	0.000	2.90	0.01	0.000	4.30	0.05	0.001
4.05	0.02	0.001	3.84	0.02	0.000	5.25	0.18	0.004
5.11	0.09	0.002	4.80	0.01	0.000	6.17	0.15	0.003
6.13	0.29	0.007	5.76	0.19	0.004	7.09	0.44	0.010
7.19	0.30	0.008	6.72	0.17	0.004	8.00	0.79	0.017
8.29	1.01	0.022	7.71	0.62	0.013	8.93	0.92	0.020
9.29	0.81	0.017	8.69	0.79	0.017	9.85	1.00	0.021
10.27	0.79	0.019	9.68	1.11	0.024	10.76	0.85	0.018
11.34	0.86	0.019	10.61	0.72	0.016	11.67	1.12	0.024
12.39	0.81	0.020	11.53	0.73	0.018	12.58	0.96	0.021
13.40	1.14	0.025	12.46	0.71	0.016	13.50	0.99	0.021
14.29	1.04	0.023	13.40	0.71	0.017	14.41	0.97	0.021
15.26	0.98	0.023	14.49	1.23	0.026	15.33	0.96	0.021
17.48	1.28	0.028	15.56	1.16	0.025	16.25	0.93	0.021
			16.49	1.09	0.024	17.16	0.99	0.021
			17.45	1.18	0.025	18.14	1.00	0.021
			18.38	1.14	0.024	19.14	0.99	0.022
			19.32	0.97	0.021	20.07	1.08	0.023
			20.31	0.99	0.021	21.02	0.93	0.020
			21.26	1.03	0.022	21.93	1.02	0.022
			22.19	1.08	0.023	22.85	1.65	0.037
			23.11	1.14	0.025	23.78	0.85	0.024

MBTP9

C1			C2			C3		
x [mm]	Lx/Tx	Lx/Tx Err.	x [mm]	Lx/Tx	Lx/Tx Err.	x [mm]	Lx/Tx	Lx/Tx Err.
1.79	0.00	0.000	9.21	0.00	0.000	2.09	0.00	0.000
2.98	0.00	0.000	10.28	0.02	0.000	3.11	0.00	0.000
4.09	0.00	0.000	11.31	0.01	0.000	4.08	0.00	0.000
5.13	0.00	0.000	12.37	0.02	0.000	5.02	0.00	0.000
6.16	0.00	0.000	12.37	0.05	0.000	5.95	0.00	0.000
7.15	0.00	0.000	13.48	0.15	0.000	6.89	0.01	0.000
8.13	0.00	0.000	18.12	0.64	0.010	7.84	0.03	0.001
9.21	0.00	0.000	24.27	1.00	0.020	8.80	0.01	0.000
10.28	0.01	0.000				9.78	0.04	0.001
11.31	0.05	0.000				10.76	0.05	0.001
12.37	0.09	0.000				11.72	0.05	0.001
13.48	0.60	0.012				12.70	0.06	0.001
14.77	0.15	0.000				13.66	0.13	0.003
15.99	0.77	0.012				14.60	0.40	0.009
17.05	0.77	0.012				15.59	0.63	0.013
18.12	0.94	0.023				16.57	0.34	0.007
19.13	0.88	0.023				17.44	0.76	0.016
20.17	0.93	0.023				18.30	0.97	0.021
21.23	0.93	0.02				19.24	0.93	0.020
22.26	1.06	0.023				20.22	1.10	0.023
23.27	1.09	0.023						
24.27	1.11	0.023						
25.28	1.07	0.023						

MBTP11

C1			C2			C3		
x [mm]	Lx/Tx	Lx/Tx Err.	x [mm]	Lx/Tx	Lx/Tx Err.	x [mm]	Lx/Tx	Lx/Tx Err.
1.17	0.00	0.000	2.42	0.00	0.000	2.62	0.05	0.000
2.05	0.00	0.000	3.37	0.00	0.000	3.57	0.01	0.000
2.98	0.00	0.000	4.32	0.00	0.000	4.67	0.01	0.000
3.90	0.02	0.000	5.23	0.00	0.000	5.67	0.08	0.002
4.83	0.00	0.000	6.16	0.00	0.000	6.75	0.04	0.001
5.77	0.03	0.001	7.14	0.02	0.000	7.85	0.06	0.001
6.71	0.02	0.000	8.02	0.08	0.002	8.89	0.08	0.002
7.66	0.04	0.001	8.93	0.32	0.007	9.97	0.34	0.007
8.60	0.19	0.004	9.99	0.47	0.010	12.61	0.54	0.012
9.50	0.49	0.012	11.03	0.29	0.006	15.20	0.72	0.016
10.39	0.38	0.009	11.96	0.67	0.014	16.37	0.90	0.020
11.33	0.56	0.012	12.89	0.71	0.015	17.50	1.07	0.023
12.29	0.77	0.018	15.17	0.80	0.017	18.49	0.92	0.020
13.15	1.02	0.023	17.45	1.02	0.022	19.65	1.00	0.021
14.09	0.94	0.022	18.58	0.96	0.020	20.77	1.03	0.022
15.11	0.89	0.021	19.73	0.97	0.021	21.83	1.03	0.022
16.09	0.97	0.025	20.68	1.14	0.024	22.93	1.05	0.022
17.03	0.88	0.036	21.72	1.03	0.022			
17.96	1.01	0.03	22.73	1.12	0.024			
18.91	1.00	0.022	23.71	0.87	0.019			
19.82	1.13	0.025	24.69	0.79	0.017			
20.70	1.00	0.026	25.69	1.12	0.024			
21.71	1.04	0.024	26.67	0.99	0.021			
22.82	1.10	0.025						

Table DR4: Infrared stimulated luminescence at 50°C (IRSL50) experimental values of Moine profile

MBAM1								
C1			C2			C3		
x [mm]	Lx/Tx	Lx/Tx Err.	x [mm]	Lx/Tx	Lx/Tx Err.	x [mm]	Lx/Tx	Lx/Tx Err.
1.44	0.00	1.445	2.13	0.00	0.00	2.19	0.93	0.02
2.86	0.00	2.865	3.18	0.00	0.00	3.12	1.00	0.02
4.15	0.00	4.155	4.02	0.00	0.00	4.03	1.04	0.02
5.25	0.00	5.259	4.85	0.00	0.00	4.88	1.21	0.03
6.23	0.00	6.243	5.69	0.00	0.00	5.76	0.86	0.02
7.14	0.00	7.152	6.99	0.01	0.00	6.72	1.13	0.02
8.04	0.00	8.049	8.95	0.02	0.00	7.65	0.85	0.02
8.99	0.00	9.000	10.71	0.03	0.00	8.51	0.64	0.01
9.86	0.00	9.877	11.66	0.39	0.02	9.37	0.66	0.01
10.67	0.00	10.686	12.71	0.20	0.01	10.22	0.76	0.02
11.65	0.00	11.667	13.83	0.20	0.00	11.18	0.62	0.01
12.67	0.00	12.689	14.72	0.63	0.02	12.17	0.65	0.01
13.62	0.00	13.643	15.74	0.51	0.01	13.06	0.83	0.02
14.57	0.00	14.597	17.24	0.87	0.02	13.99	0.72	0.02
15.51	0.00	15.532	18.74	0.73	0.02	14.90	0.79	0.02
16.40	0.00	16.423	19.64	0.94	0.02	15.79	0.69	0.02
17.28	0.00	17.307	20.58	1.22	0.04	17.10	0.76	0.02
18.29	0.00	18.324	21.50	1.00	0.02	18.38	0.81	0.02
19.61	0.00	19.641	22.40	0.94	0.04	19.26	0.54	0.01
20.78	0.00	20.816	23.30	0.84	0.02	20.16	0.47	0.01
21.68	0.00	21.715	24.22	1.03	0.02	21.05	0.45	0.01
22.67	0.00	22.709	25.09	1.04	0.02	21.91	0.23	0.01
23.63	0.00	23.671				22.80	0.16	0.00

MBAM2					
C1			C2		
x [mm]	Lx/Tx	Lx/Tx Err.	x [mm]	Lx/Tx	Lx/Tx Err.
2.66	0.00	0.000	0.63	0.06	0.043
3.81	0.00	0.000	1.90	0.00	0.000
4.73	0.00	0.001	2.92	0.00	0.000
5.62	0.00	0.000	3.96	0.00	0.000
6.48	0.00	0.000	4.93	0.00	0.000
7.37	0.01	0.001	5.91	0.00	0.000
8.26	0.02	0.000	6.98	0.00	0.000
9.16	0.00	0.000	7.98	0.00	0.000
10.03	0.02	0.001	8.95	0.00	0.000
10.93	0.03	0.001	9.92	0.05	0.001
11.85	0.02	0.000	10.91	0.04	0.001
12.74	0.04	0.001	11.90	0.09	0.008
13.63	0.05	0.001	12.94	0.07	0.002
14.53	0.20	0.004	14.02	0.14	0.003
15.65	0.45	0.010	15.10	0.43	0.009
16.71	0.61	0.013	16.12	0.65	0.014
17.62	0.79	0.018	17.13	0.79	0.017
18.56	0.92	0.020	18.20	0.92	0.020
19.44	0.96	0.024	19.18	0.97	0.021
20.35	1.03	0.023	20.15	0.97	0.021
21.28	1.02	0.023	21.16	0.83	0.018
			22.25	1.02	0.022
			23.33	1.09	0.025
			24.31	1.18	0.026

MBAM3					
C1			C2		
x [mm]	Lx/Tx	Lx/Tx Err.	x [mm]	Lx/Tx	Lx/Tx Err.
3.61	0.00	0.000	0.60	0.01	0.001
4.52	0.00	0.000	1.87	0.00	0.000
5.52	0.02	0.001	2.93	0.00	0.000
6.40	0.03	0.001	3.91	0.00	0.000
7.23	0.09	0.002	4.86	0.00	0.000
8.59	0.02	0.000	5.90	0.01	0.000
10.14	0.18	0.004	6.98	0.00	0.000
11.14	0.13	0.003	8.21	0.02	0.001
12.25	0.11	0.003	9.34	0.05	0.002
13.54	0.76	0.016			
14.75	0.89	0.020			
15.77	0.95	0.021			
16.68	1.04	0.025			
17.64	1.02	0.022			
18.53	0.95	0.021			
19.41	1.06	0.023			
20.42	0.86	0.019			
21.42	1.09	0.024			
22.38	1.03	0.022			
23.33	1.04	0.023			
24.29	1.03	0.027			
25.21	0.92	0.021			

Table DR5: Infrared stimulated luminescence at 50°C (IRSL50) experimental values of the calibration sites

MBTP7								
C1			C2			C3		
x [mm]	Lx/Tx	Lx/Tx Err.	x [mm]	Lx/Tx	Lx/Tx Err.	x [mm]	Lx/Tx	Lx/Tx Err.
0.33	0.00	0.000	0.36	0.05	0.001	0.40	0.00	0.000
1.34	0.00	0.000	1.46	0.00	0.000	1.59	0.00	0.000
2.49	0.00	0.000	2.64	0.01	0.000	2.75	0.00	0.000
3.65	0.01	0.000	3.77	0.01	0.000	3.88	0.00	0.000
4.73	0.01	0.000	4.84	0.02	0.000	5.01	0.01	0.000
5.84	0.02	0.001	5.91	0.03	0.001	6.06	0.02	0.000
6.91	0.11	0.002	6.96	0.06	0.001	7.11	0.03	0.001
7.93	0.17	0.004	7.97	0.07	0.002	8.15	0.12	0.003
8.96	0.38	0.008	8.99	0.16	0.003	9.19	0.36	0.008
10.06	0.51	0.011	9.99	0.42	0.009	10.29	0.69	0.015
11.16	0.66	0.014	11.04	0.62	0.013	11.38	0.66	0.014
12.09	0.94	0.020	12.10	0.72	0.015	12.42	0.84	0.018
13.11	0.99	0.021	13.12	0.87	0.019	13.44	0.87	0.018
14.22	1.02	0.022	14.20	1.06	0.023	14.45	0.92	0.023
15.35	1.05	0.022	15.28	1.00	0.021	15.63	0.67	0.014
16.50	0.98	0.021	16.28	1.00	0.021	16.81	1.03	0.022
17.54	1.03	0.022	17.26	1.01	0.021	17.89	1.18	0.025
18.61	1.09	0.023	18.32	1.03	0.022	18.97	1.02	0.022
19.61	1.12	0.024	19.64	0.88	0.019	20.01	0.91	0.019
20.60	1.05	0.023	20.88	1.04	0.022	21.03	0.95	0.020
21.63	0.93	0.020	21.89	1.10	0.023	22.07	0.98	0.021
22.65	0.93	0.020	22.93	1.02	0.022	23.11	0.96	0.020
23.80	0.87	0.019	23.95	0.97	0.021	24.20	0.97	0.021
			25.02	1.02	0.022			

MBTP8								
C1			C2			C3		
x [mm]	Lx/Tx	Lx/Tx Err.	x [mm]	Lx/Tx	Lx/Tx Err.	x [mm]	Lx/Tx	Lx/Tx Err.
2.00	0.00	0.000	2.00	0.00	0.000	2.33	0.00	0.000
2.95	0.00	0.000	2.95	0.00	0.000	3.34	0.01	0.000
3.92	0.00	0.000	3.92	0.00	0.000	4.41	0.02	0.000
4.93	0.00	0.000	4.93	0.00	0.000	5.44	0.08	0.002
5.93	0.00	0.000	5.93	0.00	0.000	6.49	0.04	0.001
6.90	0.01	0.000	6.90	0.01	0.000	7.56	0.05	0.001
7.87	0.09	0.002	7.87	0.09	0.002	8.61	0.06	0.001
8.87	0.32	0.007	8.87	0.32	0.007	9.63	0.07	0.002
9.85	0.64	0.013	9.85	0.64	0.013	10.62	0.09	0.002
10.81	0.81	0.017	10.81	0.81	0.017	11.60	0.08	0.002
11.77	0.80	0.017	11.77	0.80	0.017	12.56	0.57	0.012
12.74	0.99	0.021	12.74	0.99	0.021	13.49	0.61	0.013
13.72	0.93	0.020	13.72	0.93	0.020	14.48	1.01	0.021
14.67	0.84	0.018	14.67	0.84	0.018	15.53	1.44	0.031
15.86	0.89	0.019	15.86	0.89	0.019	16.76	1.16	0.025
17.06	1.11	0.024	17.06	1.11	0.024	17.94	0.89	0.019
18.01	0.83	0.018	18.01	0.83	0.018	18.92	0.92	0.019
18.98	1.06	0.023	18.98	1.06	0.023	19.95	0.81	0.017
19.93	1.12	0.02	19.93	1.12	0.024	20.99	0.88	0.019
20.88	1.12	0.024	20.88	1.12	0.024	23.03	0.99	0.021
21.83	0.97	0.020	21.83	0.97	0.020	24.05	1.00	0.021
22.78	1.06	0.022	22.78	1.06	0.022	25.08	1.05	0.022
23.73	1.09	0.023	23.73	1.09	0.023	26.11	0.85	0.018
24.66	1.00	0.021	24.66	1.00	0.021			

Table A6: Dosimetry calculations for the feldspar samples analyzed.

Sample ID	U [ppm]	Th [ppm]	K [ppm]
MBAM1	7.17 ± 0.16	25.0 ± 0.4	3.53 ± 0.05
MBAM2	7.34 ± 0.16	28.0 ± 0.5	3.85 ± 0.05
MBAM3	8.33 ± 0.18	20.0 ± 0.3	3.32 ± 0.04
MBTP1	5.69 ± 0.12	36.8 ± 0.6	2.56 ± 0.03
MBTP2	5.77 ± 0.13	20.0 ± 0.3	3.71 ± 0.05
MBTP5	7.37 ± 0.16	21.0 ± 0.4	3.68 ± 0.05
MBTP6	8.75 ± 0.19	26.0 ± 0.4	3.88 ± 0.05
MBTP9	2.76 ± 0.06	12.0 ± 0.2	5.14 ± 0.07
MBTP11	7.66 ± 0.17	19.0 ± 0.3	4.32 ± 0.07

Conversion factors has been chosen after Adamiec and Aitken (1998). Alpha-particle attenuation and Beta-particle attenuation factors have been chosen after Bell (1980) and Mejdahl (1979) respectively. Cosmic dose rates have been calculated using the method of Prescott and Hutton (1994), assuming an overburden density of 2.7 ± 0.1 g cm^{-3}. Internal K concentration is assumed to be 12 ± 0.5% for both samples. Environmental dose rates were calculated using DRAC online calculator (Durcan et al., 2015), assuming a grain size between 750 and 1000 μm and water content of 2%.

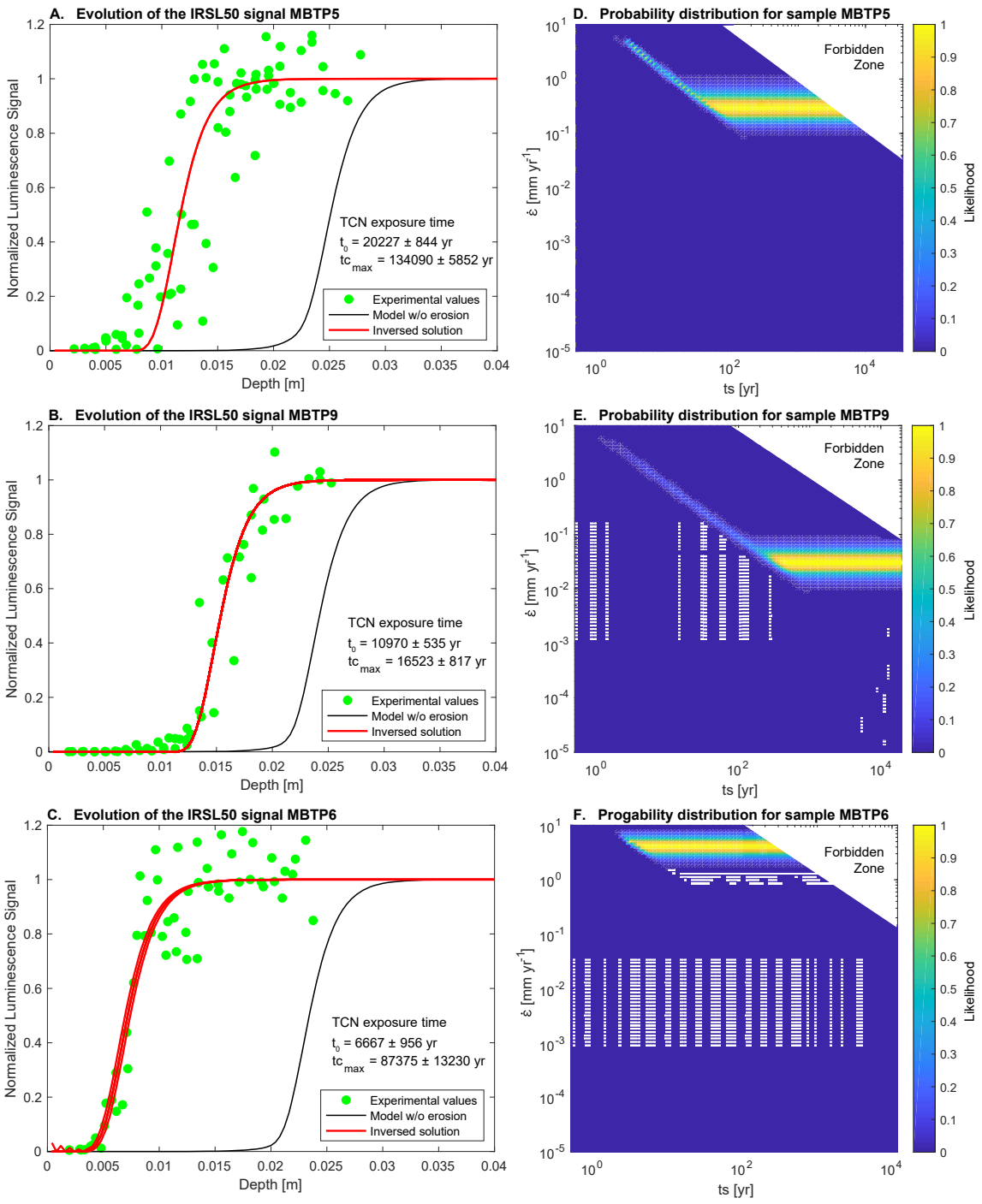

Figure A3: IRSL50 profiles and inversion results for samples MBTP5, MBTP9 and MBTP6. (a), (b) and (c) Green dots represent the measured IRSL50 profiles for samples MBTP5, MBTP9 and MBTP6 respectively. Dashed black lines represent the reference profiles and taking the TCN

exposure age with no erosion correction (t_0). Red lines represent inferred fits where the likelihood is greater 0.95. tc_{max} represents the maximum corrected TCN exposure age. (d), (e) and (f) represent the probability distributions inverted from respective insets (a), (b) and (c). The forbidden zone defines the range of solutions with high erosion rates and durations which is unable to predict the observed ^{10}Be concentration.

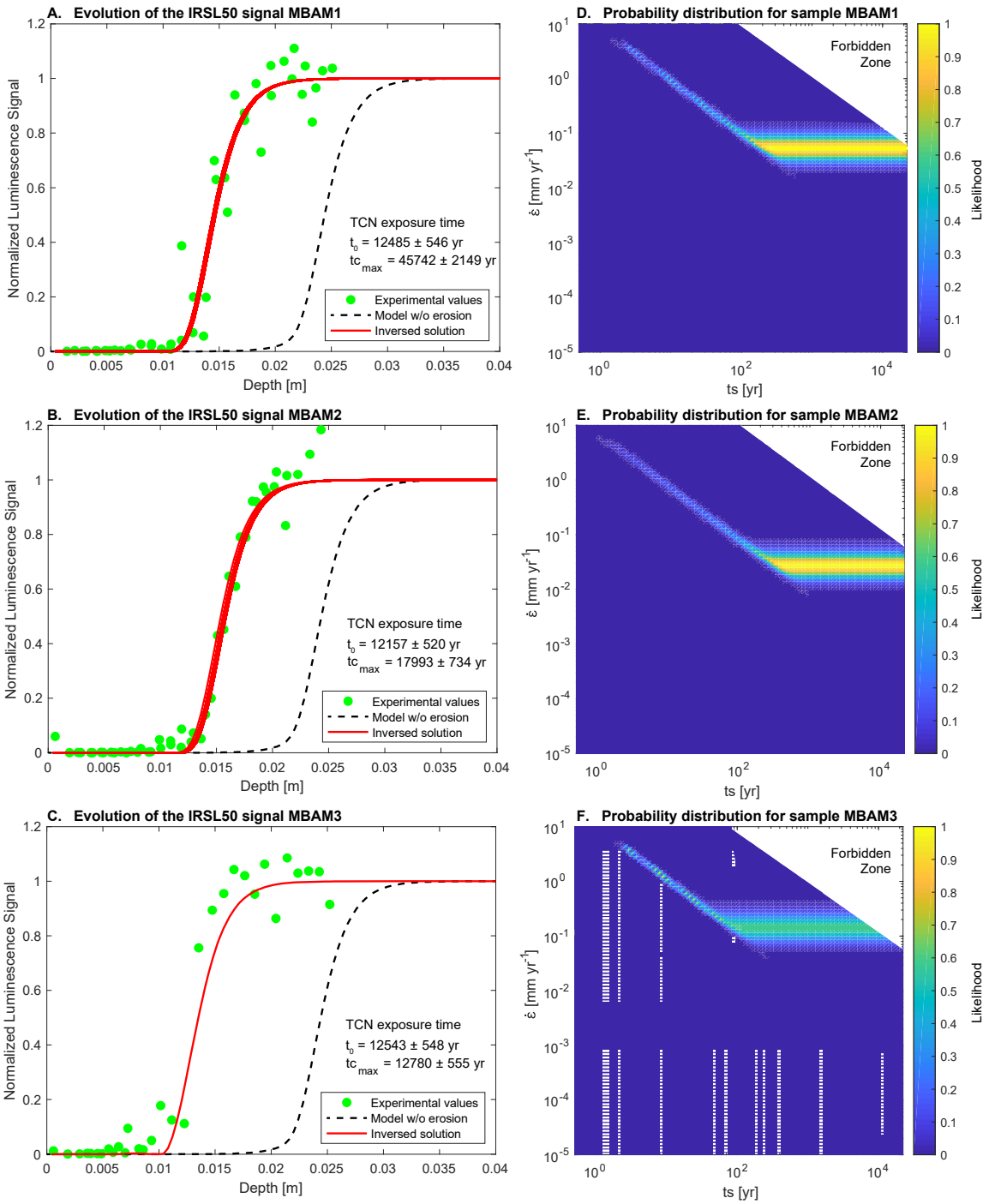

Figure A4: IRSL50 profiles and inversion results for samples MBAM1, MBAM2 and MBAM3. (a), (b) and (c) Green dots represent the measured IRSL50 profiles for samples MBAM1, MBAM2 and MBAM3 respectively. Dashed black lines represent the reference profiles and taking the TCN exposure age with no erosion correction (t_0). Red lines represent inferred fits where the

likelihood is greater 0.95. tc_{max} represents the maximum corrected TCN exposure age. (d), (e) and (f) represent the probability distributions inverted from respective insets (a), (b) and (c). The forbidden zone defines the range of solutions with high erosion rates and durations which is unable to predict the observed ^{10}Be concentration.

APPENDIX REFERENCES

Adamiec, G., & Aitken, M. J., 1998, Dose-rate conversion factors: update: Ancient TL, v. 16, no. 2, p. 37-50.

Bell, W. T., 1980, Beta source calibration: some problems associated with the utilisation of the gamma irradiation of quartz and other phosphors: Ancient TL, v. 11, p. 2-6.

Bøtter-Jensen, L., Thomsen, K.J., Jain, M., 2010, Review of optically stimulated luminescence (OSL)
instrumental developments for retrospective dosimetry: Radiation Measurement, v. 45, p. 253-257.

Claude, A., Ivy-Ochs, S., Kober, F., Antognini, M., Salcher, B., & Kubik, P. W., 2014, The Chironico landslide (Valle Leventina, southern Swiss Alps): age and evolution: Swiss Journal of Geosciences, v. 107, no. 2-3, p. 273-291.

Christl, M., Vockenhuber, C., Kubik, P. W., Wacker, L., Lachner, J., Alfimov, V., & Synal, H. A., 2013, The ETH Zurich AMS facilities: Performance parameters and reference materials. Nuclear

148 Instruments and Methods in Physics Research Section B: Beam Interactions with Materials and
149 Atoms, v. 294, p. 29-38.
150
151 Durcan, J. A., King, G. E., & Duller, G. A., 2015, DRAC: Dose Rate and Age Calculator for
152 trapped charge dating: Quaternary Geochronology, v. 28, p. 54-61.
153
154 Laj, C., Kissel, C., Beer, J., 2004, High resolution global Paleointensity Stack since 75 kyr
155 (GLOPIS-
156 75) calibrated to Absolute values. Timescales Paleomagnetic Field: Geophysical Monograph
157 Series,
158 v. 145, p. 255-265.
159
160 Lifton, N.A., Sato, T., Dunai, T.J., 2014, Scaling in situ cosmogenic nuclide production rates
161 using
162 analytical approximations to atmospheric cosmic-ray fluxes: Earth Planetary Science Letters, v.
163 386,
164 p. 149-160.
165
166 Mejdahl, V., 1979, Thermoluminescence dating: beta-dose attenuation in quartz grains:
167 Archaeometry, v. 21, no. 1, p. 61-72.
168
169 Murray, A.S., Wintle, A.G., 2000, Luminescence dating of quartz using an improved single-
170 aliquot
171 regenerative-dose protocol: Radiation measurements, v. 32, p. 57-73.
172

173 Nishiizumi, K., Imamura, M., Caffee, M. W., Southon, J. R., Finkel, R. C., & McAninch, J., 2007,
174 Absolute calibration of 10Be AMS standards. Nuclear Instruments and Methods in Physics
175 Research Section B: Beam Interactions with Materials and Atoms, v. 258, no. 2, p. 403-413.
176
177 Pavon-Carrasco, F.J., Osete, M.L., Torta, J.M., De Santis, A., 2014, A geomagnetic field model
178 for
179 the Holocene based on archaeomagnetic and lava flow data: Earth and Planetary Science Letters,
180 v. 388, p. 98-109.
181
182 Prescott, J. R., & Hutton, J. T., 1994, Cosmic ray contributions to dose rates for luminescence and
183 ESR dating: large depths and long-term time variations: Radiation measurements, v. 23, no. 2-3, p.
184 497-500.
185
186 Uppala, S.M., Kallberg, P.W., Simmons, A.J., Andrae, U., Bechtold, V.D.C., Fiorino, M., Gibson,
187 J.K., Haseler, J., Hernandez, A., Kelly, G.A., Li, X., Onogi, K., Saarinen, S., Sokka, N., Allan,
188 R.P., Andersson, E., Arpe, K., Balmaseda, M.A., Beljaars, A.C.M., Van De Berg, L., Bidlot, J.,
189 Bormann, N., Caires, S., Chevallier, F., Dethof, A., Dragosavac, M., Fisher, M., Fuentes, M.,
190 Hagemann, S., Holm, E., Hoskins, B.J., Isaksen, L., Janssen, P.A.E.M., Jenne, R., Mcnally, A.P.,
191 Mahfouf, J.-F., Morcrette, J.- J., Rayner, N.A., Saunders, R.W., Simon, P., Sterl, A., Trenberth,
192 K.E., Untch, A., Vasiljevic, D., Viterbo, P., Woollen, J., 2005, The ERA-40 re-analysis: Quaterly
193 Journal of the Royal Meteorological Society, v. 131, p. 2961-3012.
194
195 Wallinga, J., Murray, A., Wintle, A., 2000, The single-aliquot regenerative-dose (SAR) protocol
196 applied to coarse-grain feldspar: Radiation Measurements, v. 32, p. 529-533.
197